

---

## Chandra Studies of Nonthermal Emission from Supernova Remnants and Pulsar Wind Nebulae

---

Patrick Slane

*Harvard-Smithsonian Center for Astrophysics*

*60 Garden Street*

*5A Cambridge, MA 02138, USA*

---

### Abstract

While supernova remnants (SNRs) have long been considered prime candidates as sources of cosmic rays, it is only recently that X-ray observations have identified several shell-type SNRs dominated by nonthermal emission, thus revealing shock-accelerated electrons with energies extending far beyond the typical thermal spectrum. Two of these SNRs have been detected as sources of VHE  $\gamma$ -rays. In other remnants, discrepancies between the shock velocity and the electron temperature point to a strong cosmic ray component that has thrived at the expense of the thermal gas. Modeling of the radio, X-ray, and  $\gamma$ -ray emission provides constraints on particle acceleration as well as the properties of the medium in which the mechanism prospers.

Crab-like pulsar wind nebulae (PWNe) are characterized by a termination shock at which the wind is forced to join the slow expansion of the outer nebula. These shocks also act as sites in which particles are boosted to high energies; the X-ray emission from the Crab Nebula, as well as the inverse Compton radiation observed as VHE  $\gamma$ -rays, imply electrons with energies in excess of  $\sim 100$  TeV. Recent X-ray observations have begun to reveal these shock zones in the Crab and other PWNe, and are now allowing us to constrain the nature of pulsar winds as well as the flow conditions in the outer nebulae. Here I present a brief overview of recent studies with the *Chandra X-ray Observatory* in which the properties of these shock acceleration regions are finally being revealed.

### 1. Introduction

Supernova remnants and their associated pulsars are sites in which strong shocks act to accelerate particles to extremely high energies. The connection between SNRs and the energetic cosmic rays that pervade the Galaxy has long been assumed, for example; shock acceleration by the SNR blast wave provides ample energy for the production of multi-TeV particles, and recent observations

of nonthermal X-ray and VHE  $\gamma$ -ray emission from several SNRs has confirmed the presence of electrons at these high energies. At the same time, models for the structure of PWNe predict particle acceleration at the wind termination shock, and recent X-ray observations have begun to probe these acceleration sites. These X-ray measurements provide constraints on the expected higher energy emission processes, and are thus of considerable interest in the context of VHE  $\gamma$ -ray astronomy. Here I review recent *Chandra* studies of nonthermal X-ray emission in SNRs and PWNe, with particular emphasis on the evidence for particle acceleration to very high energies.

## 2. Nonthermal X-rays and Particle Acceleration in SNRs

The radio synchrotron emission from SNRs is testimony to the presence of energetic particles. However, this corresponds to electron energies far below the “knee” of the cosmic ray spectrum at  $\sim 10^{15}$  eV:

$$E_{\text{GeV}} \approx \left[ \frac{\nu}{16 \text{ MHz}} B_{\mu}^{-1} \right]^{1/2} \quad (1)$$

where  $\nu$  is the frequency of the radio emission and  $B_{\mu}$  is the magnetic field strength in  $\mu\text{G}$ . X-ray observations allow us to probe much higher energy particles, and also characterize the thermodynamic states of SNRs and infer the dynamics of their evolution. For an ideal gas, the thermal postshock temperature is

$$T = \frac{3\mu m}{16k} V_s^2 \quad (2)$$

where  $V_s$  is the shock speed,  $m$  is the proton mass, and  $\mu$  is the mean molecular weight of the gas ( $\mu \approx 0.6$ ). This shock-heated gas yields the familiar X-ray emission, characterized by a thermal bremsstrahlung spectrum accompanied by strong emission lines.

In addition to thermal heating of the swept-up gas, some fraction of the shock energy goes into nonthermal production of relativistic particles through diffusive shock acceleration. The maximum particle energy in such a scenario can be limited by radiative losses, the finite age of the SNR, or particle escape from the accelerating region. If the relativistic particle component of the energy density becomes comparable to that of the thermal component, the shock acceleration process can become highly nonlinear. The gas becomes more compressible, which results in a higher density and enhanced acceleration. When the acceleration is very efficient, the relationship between the shock velocity and the mean postshock temperature is no longer well approximated by Eq. 2; the acceleration process depletes thermal energy, and the temperature for a given shock velocity drops

below that expected in the test particle case (Decourchelle et al. 2002). This process has been considered in detail by Baring et al. (1999) who present a model for the radio to  $\gamma$ -ray emission. The broadband spectra of SNRs depend highly on ambient conditions, and X-ray studies of these SNRs reveal these conditions and can provide spectral measurements which strongly constrain the models.

In the simplest picture, the passage of material through the SNR shock results in electrons and ions being boosted to the velocity of the shock. Because of the mass difference, this means that the electrons and ions are not initially in temperature equilibrium. The maximum timescale for equilibration is that provided by Coulomb interactions, but plasma processes may reduce this considerably. The state of equilibration is important, because while the dynamics of SNR evolution are dominated by the ions (which carry the bulk of the momentum), it is the electrons that produce the X-ray emission we observe. Thus, when temperature measurements are used to infer the shock velocity, for example, the state of temperature equilibration is exceedingly important.

As an example, the blast wave speed inferred from an expansion study comparing a *Chandra* image of 1E 0102.2–7219 (Figure 1, left), with high resolution images taken with *Einstein* and *ROSAT* indicates a post-shock temperature which is much higher than the observed electron temperature (Hughes et al. 2001). In this case, the discrepancy appears to be larger than can be accounted for assuming Coulomb equilibration, suggesting that a significant fraction of the shock energy has gone into cosmic ray acceleration rather than thermal heating of the postshock gas. Higher resolution X-ray expansion studies of 1E 0102.2–7219 (and other young SNRs) are needed to confirm this scenario, but the notion that particle acceleration is efficient enough in some SNRs to significantly affect their dynamics has strong foundations from recent studies of other SNRs. As we discuss below, direct evidence of very energetic electrons now exists for a handful of shell-type SNRs. In addition to the two SNRs which we discuss in the following sections (and also G266.2–1.2; Slane et al. 2001), for which synchrotron radiation dominates the X-ray emission, evidence for energetic particles in the form of nonthermal filaments or hard tails in the X-ray spectra have also been observed for Cas A (Allen et al. 1997, Hughes et al. 1999, Vink et al. 1999), RCW 86 (Borkowski et al. 2001, Rho et al. 2002), and other SNRs.

### 2.1. SN 1006

The first evidence of multi-TeV particles directly associated with a shell-type SNR was uncovered in studies of SN 1006 with the ASCA observatory (Koyama et al. 1995). While spectra from the central regions of the SNR show distinct line emission associated with shock-heated gas, the emission from the bright

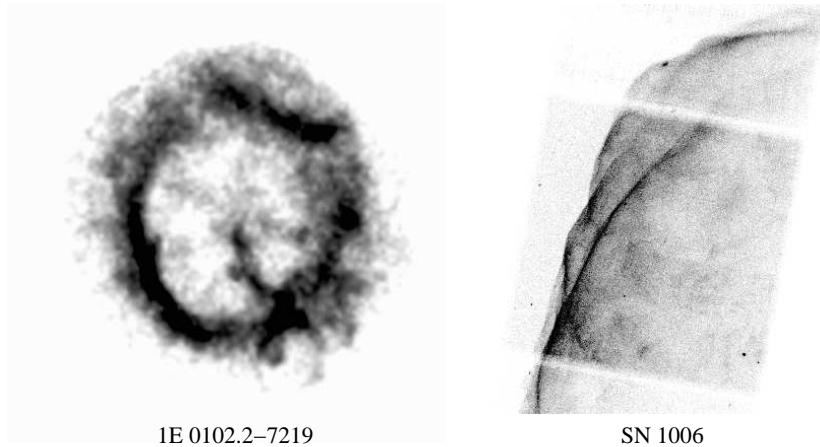


**Fig. 1.** Left: *Chandra* image of 1E 0102.2–7219, a young oxygen-rich SNR in the SMC. A comparison of the expansion rate and shock temperature indicates that considerable energy has gone into particle acceleration. Right: *Chandra* image of the northeast limb of SN 1006. The diffuse X-ray emission in the interior regions is thermal emission from the hot postshock gas. The outer limb, which is observed to consist of bright filaments, is dominated by synchrotron from extremely energetic electrons.

limbs of the remnant was shown to be completely dominated by synchrotron emission. Reynolds (1998) modeled the emission as the result of diffusive shock acceleration in a low density medium with the magnetic field orientation providing the distinct “bilateral” morphology. Subsequent observations with the CANGAROO telescope revealed VHE  $\gamma$ -ray emission from one limb of the SNR (Tanimori et al. 1998), thus confirming the presence of extremely energetic particles. The low ambient density of this remnant, which resides well above the Galactic Plane, is insufficient to explain the  $\gamma$ -ray emission as the result of  $\pi^0$  decay from proton-proton collisions. Rather, the emission results from inverse-Compton scattering of microwave background photons off the energetic electron population in SN 1006 (but see Berezhko – these proceedings – for an alternative picture). Using joint spectral fits to the radio as well as thermal and nonthermal X-ray emission, Dyer et al. (2001) conclude that the total energy in relativistic particles is  $\sim 100$  times the energy in the magnetic field, confirming the notion that the nonthermal particle component contributes significantly to the dynamics of the blast wave evolution.

*Chandra* observations of SN 1006 (Figure 1, right) reveal sharp filamentary structure along the SNR rim. Diffuse emission beyond these filaments is observed, presumably indicating the upstream diffusion of particles accelerated in the shocks. The upstream scale length of these nonthermal filaments appears

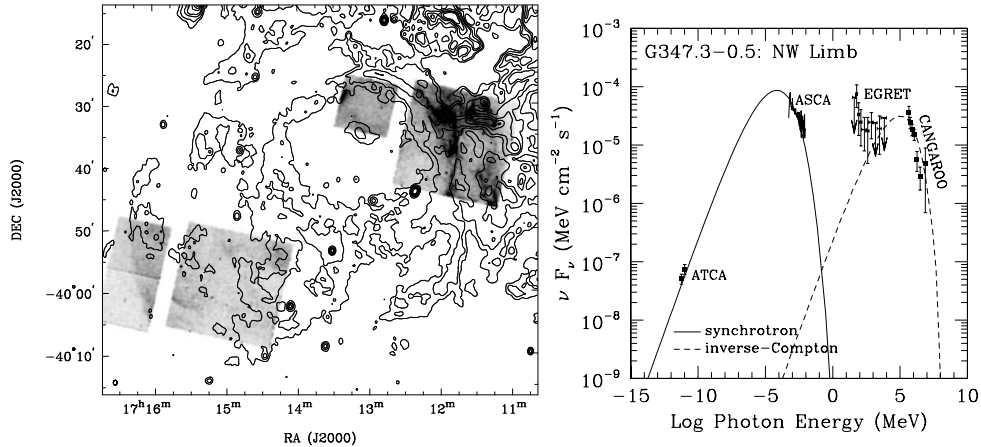


**Fig. 2.** Left: Radio contours of G347.3–0.5 from the ATCA, along with *Chandra* images of the NW and SE regions of the SNR. X-ray filaments in the NW follow radio arcs; VHE  $\gamma$ -ray emission is detected from this region. Right: Model of the broad-band emission from G347.3–0.5 assuming a power law distribution of electrons with an exponential cutoff ( $E_{\text{max}} \sim 3$  TeV) and a magnetic filling factor comprising only  $\sim 0.7\%$  of the inverse-Compton emitting region (Lazendic et al. 2003).

to be considerably smaller than expected for standard diffusive shock acceleration, however (Bamba et al. – these proceedings), possibly indicating an upstream field nearly parallel to the plane of the shock and a downstream magnetic field strength ( $\sim 50 \mu\text{G}$ ) considerably higher than that previously estimated (e.g. Reynolds 1998). A program to map SN 1006 in its entirety with *Chandra* is underway. This will form a baseline for future expansion measurements that will bear heavily on these questions.

## 2.2. G347.3–0.5 (RX J1713.7–3946)

ASCA observations of G347.3–0.5 (Koyama et al. 1997, Slane et al. 1999) established this as the second member of the class of shell-type SNRs for which the X-ray flux is dominated by synchrotron radiation. Unlike SN 1006, this SNR appears to have evolved in the vicinity of dense molecular clouds (Slane et al. 1999) with which the shock may now be interacting. CANGAROO observations (Muraishi et al. 2000) reveal VHE  $\gamma$ -ray emission from the vicinity of the north-west rim, which is brightest in X-rays. Combining radio measurements from the ATCA with the X-ray and  $\gamma$ -ray results, Ellison, Slane, & Gaensler (2001) used diffusive shock acceleration models to conclude that the radio and X-ray emission results from synchrotron radiation from a nonthermal electron population accelerated by the forward shock, and that the  $\gamma$ -ray emission can be self-consistently modeled as inverse-Compton emission. Combined with limits on the ambient

density based on the lack of thermal X-ray emission, the models indicate very efficient particle acceleration with  $> 25\%$  of the shock kinetic energy going into relativistic ions. A comparison of *Chandra* observations of the northwest rim with high resolution radio maps from the ATCA shows good overall agreement with the radio and X-ray morphology in this region (Figure 2, left), consistent with the interpretation that the emission comes from the same electron population (Lazendic, et al. 2003).

The nearby unidentified EGRET source 3EG J1714-3857 has been suggested as being associated with G347.3-0.5, possibly resulting from the decay of neutral pions produced in the collision of accelerated ions with the nearby molecular clouds (Butt, et al. 2001), although this would appear inconsistent with the X-ray measurements unless the emission originates from a distinct spatial region. Most recently, Enomoto et al. (2002) have presented new CANGAROO data which, they argue, establish  $\pi^0$ -decay as the mechanism by which the TeV  $\gamma$ -rays are produced. However, the predicted spectrum over-predicts emission from the EGRET band by a large margin (Reimer et al. 2002, Butt et al. 2002), making the claim for direct observation of ion acceleration appear problematic.

The CANGAROO spectrum can be modeled as inverse-Compton emission from the same electron spectrum that produces the synchrotron radiation, while still falling below the EGRET limits, if the strong magnetic field region in which the synchrotron emission comprises only a small fraction of the total volume over which the inverse-Compton emission is produced (Figure 2, right; Lazendic et al. 2003). The resulting magnetic field filling factor is only  $\sim 0.7\%$ , which is quite small although the long diffusion lengths for the energetic particles certainly make the inverse-Compton emitting region considerably larger than that of the compressed magnetic field region where the bulk of the synchrotron emission arises. The field strength in the synchrotron filaments must be  $\sim 50\mu\text{G}$ , which is very high, though similar to values found in maser-producing regions of molecular clouds. Uchiyama et al. (2002) have also modeled the synchrotron emission in G347.3-0.5 to assess the required magnetic field conditions. For a distance of 6 kpc, they derive  $B \sim 50\mu\text{G}$  – similar to that obtained in our analysis – but require that this field be similar in the filamentary and diffuse emission regions. This leads to the conclusion that the spectral cutoff in the diffuse emission regions is due to radiative losses while that in the filaments is due to diffusive escape of the particles. The resulting inverse-Compton emission falls far below the observed CANGAROO flux, thus requiring some other mechanism to produce the TeV  $\gamma$ -ray emission.

### 3. Energetic Particles from Pulsars and Their Wind Nebulae

Our basic understanding of “Crab-like” SNRs stems from the picture presented by Rees & Gunn (1974), and expanded upon by Kennel & Coroniti (1984a,b) in which an energetic wind is injected from a pulsar into its surroundings. As illustrated schematically in Figure 3, the basic structure of a pulsar wind nebula is regulated by the input power from the pulsar and the density of the medium into which the nebula expands; the pulsar wind inflates a magnetic bubble which is confined in the outer regions by the expanding shell of ejecta or interstellar material swept up by the SNR blast wave. The boundary condition established by the expansion at the nebula radius  $r_N$  results in the formation of a wind termination shock at which the highly relativistic pulsar wind is decelerated to  $v \approx c/3$  in the postshock region, ultimately merging with the particle flow in the nebula. The shock forms at the radius  $r_w$  at which the ram pressure of the wind is balanced by the internal pressure of the pulsar wind nebula:

$$r_w^2 = \dot{E}/(4\pi\eta cp) \quad (3)$$

where  $\dot{E}$  is the rate at which the pulsar injects energy into the wind,  $\eta$  is the fraction of a spherical surface covered by the wind, and  $p$  is the total pressure outside the shock.

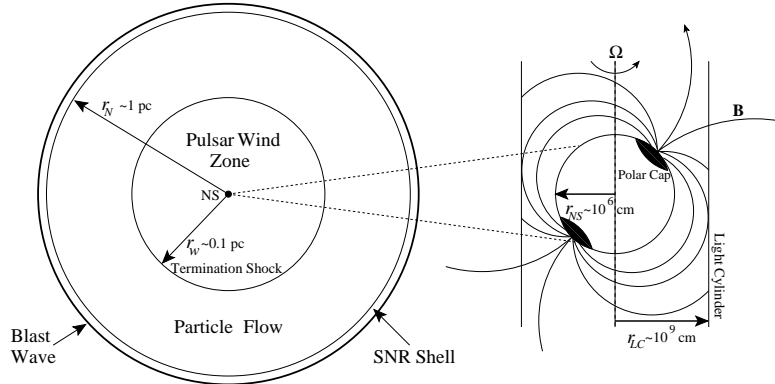


**Fig. 3.** Schematic view of a pulsar and its wind nebula. See the text for a complete description. (Note the logarithmic size scaling in the PWN figure when comparing with images shown elsewhere in the text.)

The dynamics of the particle flow yield  $\gamma \sim 10^6$  for the electrons in the postshock region (Arons & Tavani 1994). However, for typical magnetic field strengths the observed X-ray emission requires  $\gamma > 10^8$ . Particle acceleration at the termination shock apparently boosts the energies of the wind particles by a factor of 100 or more, to energies in excess of  $\sim 50$  TeV. Arons & Tavani (1994;

see also Arons 2002) note that this process cannot proceed by normal diffusive shock acceleration because the magnetic field at the termination shock must be nearly perpendicular to the flow. Rather, they argue that the  $e^\pm$  acceleration is the result of resonant cyclotron absorption of low frequency electromagnetic waves emitted by ions gyrating in the compressed  $B$ -field of the hot post-shock gas. Ultimately, the pressure in the nebula is believed to reach the equipartition value; a reasonable pressure estimate can be obtained by integrating the radio spectrum of the nebula, using standard synchrotron emission expressions, and assuming equipartition between particles and the magnetic field. Typical values yield termination shock radii of order 0.1 pc, which yields an angular size of several arcsec at distances of a few kpc.

The pulsar wind can be characterized in terms of  $\dot{E}$  and the parameter  $\sigma$  representing the ratio of Poynting flux to particle flux. For the Crab Nebula, Kennel & Coroniti (1984a) find that small values of  $\sigma$  ( $\sim 10^{-3}$ ) are required, indicating a particle-dominated wind. Yet current understanding of pulsar outflows predicts  $\sigma \gg 1$  where the wind is launched (Arons 2002). Somehow, between the pulsar light cylinder and the wind termination shock the balance between the electromagnetic energy and the kinetic energy of the flow changes dramatically. The ability to identify the termination shock and measure the emission parameters in the immediate region is now providing constraints on the nature of the wind that may ultimately help unravel this problem. Below I summarize recent X-ray investigations that have finally begun to probe this important shock region in which particle acceleration is apparently taking place.

### 3.1. Crab Nebula

The Crab Nebula is the best known of the class of pulsar wind nebulae and has inspired much of the theoretical work on PWNe. Powered by an energetic central pulsar, it emits synchrotron radiation from radio wavelengths up beyond the hard X-ray band. Optical wisps are observed in the inner nebula, at a position interpreted as the pulsar wind termination shock (Hester 1995), and high resolution X-ray observations (Figure 4, left) reveal a distinct ring of emission in this same region as well as a jet emanating from the pulsar (Weisskopf et al. 2000). Moreover, monitoring observations of the Nebula (Hester 1995, Mori et al. 2002) show that these and other detailed features are highly dynamic. The discovery of radio wisps in inner ring region (Bietenholz et al. 2002) suggests that the acceleration site may be the same for the entire population of electrons that produce the broad-band synchrotron emission.

In addition to the jet and inner ring, the X-ray image reveals an outer toroidal structure that presumably lies in the equatorial plane, as well as fine



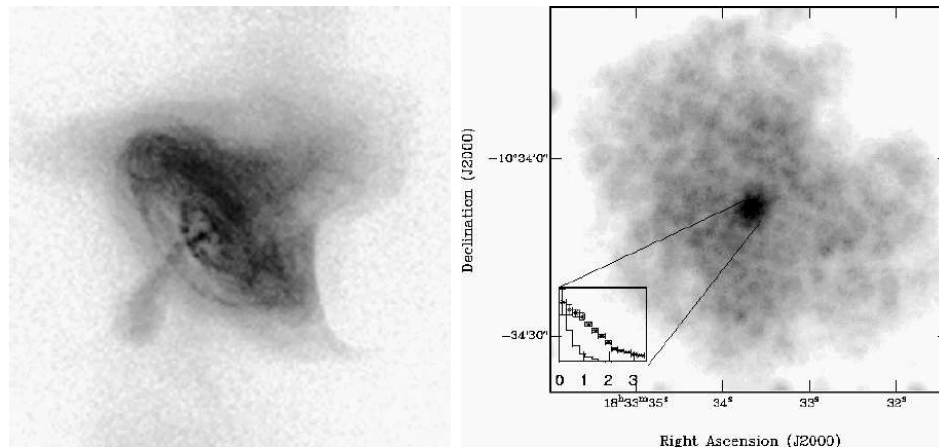


**Fig. 4.** Left: *Chandra* image of the Crab Nebula showing the toroidal structure, the jet, and the inner ring corresponding to the pulsar termination shock. Right: *Chandra* image of G21.5-0.9, a PWN whose pulsar has not yet been detected. The bright central X-ray source is resolved in this image (see inset); the  $\sim 2 - 3$  arcsec extent is consistent with the expected size of the termination shock zone.

structure correlated with optical polarization measurements, indicating that the structures trace the magnetic field. The early models of Rees & Gunn (1974) and Kennel & Coroniti (1984a,b) predict these basic properties as the result of a wound-up magnetic field, the large-scale confinement of the Nebula by the (unseen) supernova ejecta, and the termination of the pulsar wind flow by an inner shock. This picture leads to the inference of a low- $\sigma$  wind described above. As we describe below, recent observations of PWNe have begun to show many similar features, indicating that our basic picture – while still poorly understood in detail – can at least be said to apply to a “class” of objects.

### 3.2. G21.5–0.9

G21.5–0.9 is a compact SNR that exhibits strong linear polarization, a flat spectrum, and centrally peaked emission in the radio band. The SNR has a lower  $L_x/L_r$  ratio than the Crab; it is a factor of  $\sim 9$  less luminous in the radio and a factor of  $\sim 100$  less in X-rays. To date, there has been no detection of a central pulsar. However, *Chandra* observations by Slane et al. (2000) reveal a compact source of emission at the center of the remnant as well as a radial steepening of the spectral index consistent with synchrotron burn-off of high energy electrons injected from a central source. Using an empirical relationship between the total X-ray luminosity of the PWN with the spin-down power of the pulsar powering the nebula (Seward & Wang 1988) suggests the presence of a pulsar with  $\dot{E} = 10^{37.5}$  erg s $^{-1}$ , although Chevalier (2000) argues that the spectral variations in

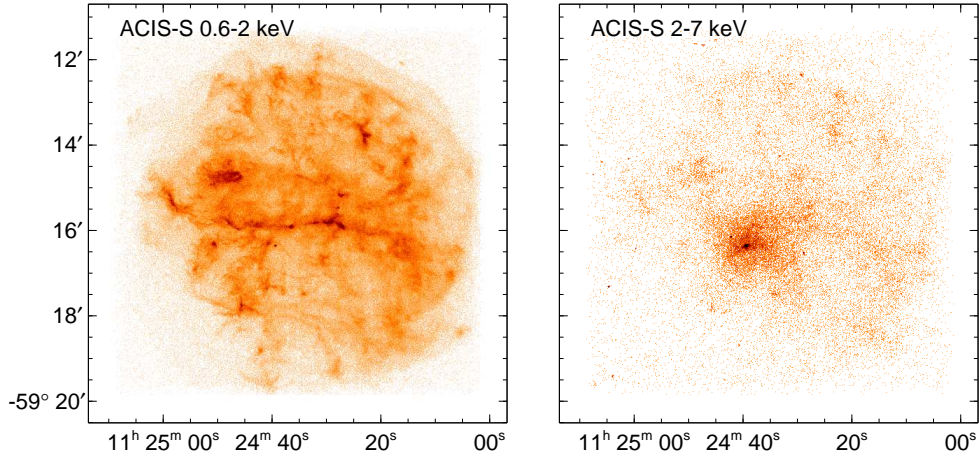


**Fig. 5.** *Chandra* ACIS-S X-ray images of G292.0+1.8 in soft (left: 0.6–2 keV) and hard (right: 2–7 keV) X-ray bands. The hard band shows a diffuse, plerionic nebula containing a central point-like source.

the nebula imply more efficient conversion of  $\dot{E}$  into X-ray emission, and suggests that  $\dot{E} \approx 10^{36.7}$  erg s $^{-1}$  is more likely for the pulsar in this PWN. Detection of pulsations from the central source are required to address this further. Using the larger  $\dot{E}$  estimate along with pressure estimates from the radio spectrum, Eq. 3 predicts a wind termination shock at a radius of  $\sim 1.5\eta^{-1/2}$  arcsec from the pulsar, assuming a distance of 5 kpc. As indicated in the inset to Figure 4, the brightness profile of the compact X-ray source in G21.5–0.9 is broader than that for a point source. The  $\sim 2''$  extent of the source is consistent with the expected size of the termination shock zone.

Slane et al. (2000) also report the presence of a faint extended shell of emission surrounding G21.5–0.9 whose featureless spectrum may be associated with energetic particles accelerated by the SNR blast wave, similar to those observed for SN 1006 and other SNRs as described in Section 2.

### 3.3. PSR J1124-5916/G292.0+1.8

G292.0+1.8 is a member of the “oxygen-rich” class of SNRs with optical emission revealing the presence of ejecta whose tell-tale composition points to a massive star progenitor. Previous studies have shown that the X-ray emission is dominated by ejecta, and have revealed a region of hard emission indicative of a pulsar-driven nebula. *Chandra* observations reveal an unprecedented example of a composite SNR showing both such components (Hughes et al. 2001, Park et al. 2002). Figure 5 (left) shows a soft X-ray image of the remnant. The bulk of the interior emission is dominated by ejecta, and spectra from discrete

regions suggest large-scale variations in ionization state and elemental abundance within the ejecta. The bar-like structure running across the center, along with the thin filamentary structure encircling most of the SNR, has solar abundances indicative of material swept up by the forward shock. The hard-band image in Figure 5 (right) reveals a neutron star with a surrounding pulsar wind nebula, similar in size to the Crab. Recent radio observations (Camilo et al. 2002) have identified a young pulsar (PSR J1124-5916) with a 135 ms rotation period that appears to be the counterpart. The *Chandra* image of the compact X-ray source is marginally extended, with a size consistent with that expected for the termination shock zone of the pulsar wind.

#### 4. Summary

The strong shocks in SNRs and PWNe have long been regarded as sites where particles are accelerated to extremely high energies. SNRs, in particular, are leading candidates as the source of cosmic rays up to the knee of the spectrum. X-ray emission from PWNe also require particles with higher energies than expected in the postshock flow of the pulsar wind, indicating efficient acceleration at the termination shock. X-ray observations have now begun to provide direct evidence of the energetic particles and shock structures where this such acceleration takes place. Through studies of the dynamics and nonthermal X-ray emission from SNRs, and of the wind termination shocks and associated particle outflows in PWNe, strong constraints are being placed on models of the particle acceleration process. High resolution X-ray observations promise continued advances in this area, through measurements of SNR nonthermal emission and expansion rates, and the inner structure of PWNe. In addition,  $\gamma$ -ray observations with current and upcoming Čerenkov telescopes, as well as future space-borne observatories, hold considerable promise for probing these sites of extremely energetic particles.

#### Acknowledgments

I would like to thank Bryan Gaensler, Jack Hughes, Don Ellison, Jasmina Lazendic, and Steve Reynolds for their contributions as collaborators on much of the above work. I also thank the organizers of this meeting for their kind invitation to present this work. This research was funded in part by NASA Contract NAS8-39073 and Grants NAG5-9281 and GO0-1117A.

#### References

1. Allen, G. E. et al. 1997, ApJ, 487, L97

2. Arons, J. 2002, in “Neutron Stars in Supernova Remnants,” ASP Conference Series, Vol. 271, eds P. O. Slane and B. M. Gaensler, p. 71
3. Arons, J. & Tavani, M. 1994, *ApJS*, 90, 797
4. Baring, M. G. et al. 1999, *ApJ*, 513, 311
5. Bietenholz, M. F., Frail, D. A., & Hester, J. J. 2001, *ApJ*, 560, 254
6. Borkowski et al. 2001, *ApJ*, 550, 334
7. Butt, Y., et al. 2001, *ApJ*, 562, L167
8. Butt, Y., et al. 2002, *Nature*, 418, 499
9. Camilo et al. 2002, *ApJ*, 567, L71
10. Chevalier, R. A. 2000, *ApJ*, 539, L45
11. Decourchelle, A., Ellison, D. C., & Ballet, J. 2002, *ApJ*, 543, L57
12. Dyer, K. K. et al. 2001, *ApJ*, 551, 439
13. Ellison, D. C., Slane, P., & Gaensler, B. M. 2001, *ApJ*, 563, 191
14. Enomoto, R. et al. 2002, *Nature*, 416, 823
15. Hester, J. J. et al. 1995, *ApJ*, 448, 240
16. Hughes, J. P. et al. 1999, *ApJ*, 528, L109
17. Hughes, J. P. et al. 2001, *ApJ*, 559, L153
18. Hughes, J. P., Rakowski, C. E. & Decourchelle, A. 2001, *ApJ*, 543, L61
19. Kennel, C. F. & Coroniti, F. V. 1984a, *ApJ*, 283, 694
20. Kennel, C. F. & Coroniti, F. V. 1984b, *ApJ*, 283, 710
21. Koyama, K. et al. 1995, *Nature*, 378, 255
22. Koyama, K. et al. 1997, *PASJ*, 49, L7
23. Lazendic, J. et al. 2003, *ApJ*, submitted
24. Mori, K. et al. 2002, in “Neutron Stars in Supernova Remnants,” ASP Conference Series, Vol. 271, eds P. O. Slane and B. M. Gaensler, p. 157
25. Muraishi, T. et al. 2000, *A&A*, 354, L57
26. Park et al. 2002, *ApJ*, 564, L39
27. Rees, M. J. & Gunn, R. E. 1974, *MNRAS*, 167, 1
28. Reimer, O. et al. 2002, *A&A*, 390, L43
29. Reynolds, S. P. 1998, *ApJ*, 493, 375
30. Seward, F. D. & Wang, Z.-R. 1988, *ApJ*, 332, 199
31. Slane, P. et al. 1999, *ApJ*, 525, 357
32. Slane, P. et al. 2000, *ApJ*, 533, L29
33. Slane, P. et al. 2001, *ApJ*, 548, 814
34. Tanimori, T. et al. 1998, *ApJ*, 497, L25
35. Vink, J. et al. 1999 *A&A*, 344, 289
36. Weisskopf, M. C. et al. 2000, 536, L81